Identifying the neutrino mass hierarchy with supernova neutrinos

M. Kachelrieß and R. Tomàs

Max-Planck-Institut für Physik (Werner-Heisenberg-Institut), München

October 18, 2004

Abstract

The high-statistics observation of the neutrino signal from a future galactic supernova (SN) may be used to discriminate between different neutrino mixing scenarios. Since the flavor-dependent differences of the emitted neutrino spectra are small and rather uncertain, such a discrimination has to rely on observables independent of poorly known SN parameters. We discuss two complementary methods that allow for the positive identification of the mass hierarchy without knowledge of the emitted neutrino fluxes, provided that the 13-mixing angle is "large" ($\sin^2 \vartheta_{13} \gg 10^{-5}$). These two approaches are the observation of a modulation in the neutrino spectra due to Earth matter effects or due to the passage of shock waves through the SN envelope. If the value of the 13-mixing angle is unknown, using additionally the information encoded in the prompt neutronization ν_e burst might be sufficient to fix both the neutrino hierarchy and to decide whether ϑ_{13} is "small" or "large."

1 Introduction

Despite the enormous progress of neutrino physics in the last decade, many open questions remain to be solved. Among them are two, the mass hierarchy – normal versus inverted mass spectrum – and the value of the 13-mixing angle ϑ_{13}, where the observation of neutrinos from a core-collapse supernova (SN) could provide important clues [1, 2, 3]. The proliferation of existing or proposed large neutrino detectors has considerably increased the confidence that such a SN neutrino signal will eventually be observed with

high-statistics. However, in contrast to terrestrial experiments, large uncertainties associated with the neutrino fluxes produced inside the SN makes a straight-forward extraction of the neutrino mixing parameters impossible. While the different interaction strength of ν_e, $\bar{\nu}_e$ and $\nu_x = \{\nu_{\mu,\tau}, \bar{\nu}_{\mu,\tau}\}$ with matter guaranties that their fluxes are not identical, the exact extent of these differences varies in different simulations. Therefore, only features in the detected neutrino spectra that are independent of unknown SN parameters should be used in such an analysis.

The two most promising sources for such features are the detection of modulations in the neutrino spectra caused by the Earth matter or by the passage of shock waves through the SN envelope. In the first case, matter effects on SN neutrinos traversing the Earth give rise to specific frequencies in the energy spectrum of these neutrinos, which are analytically known and depend only on the neutrino properties and the distance traveled through the Earth [4, 5]. In the other case, the passage of the SN shock waves through the density region corresponding to resonant neutrino oscillations with the atmospheric neutrino mass difference imprints specific time- and energy-dependent modulations on the neutrino energy spectrum [6, 7], difficult to be mimicked by other effects. Only the amplitude of both modulations, and thus the statistical confidence to detect them, depends on how different the emitted neutrino fluxes are, while the specific shape of the modulations is independent from the fluxes.

Case	Hierarchy	$\sin^2\vartheta_{13}$	Earth	Shock	ν_e burst
A	Normal	$\gtrsim 10^{-3}$	Yes	No	No
B	Inverted	$\gtrsim 10^{-3}$	No	Yes	Yes
C	Any	$\lesssim 10^{-5}$	Yes	No	Yes

Table 1: The presence of Earth-matter and shock wave effects in the $\bar{\nu}_e$ spectra and the ν_e burst for different neutrino mixing scenarios.

In the following sections we will concentrate on three different neutrino mixing schemes (A, B, C), cf. Tab. 1, where modulations by Earth or SN shock effects are clearly separated. For an inverted hierarchy and intermediate values of the 13-mixing angle, $10^{-5} \lesssim \sin^2\vartheta_{13} \lesssim 10^{-3}$, both effects can be present. In this case, modulations by Earth and SN shock effects even offer the possibility to restrict the range of ϑ_{13}.

If at the time of the SN detection the value of ϑ_{13} is known to be "large," then the neutrino mass hierarchy can be identified observing the modulations induced either by the SN shock wave propagation (case B in Tab. 1) or by the Earth matter effects (case A). If the value of ϑ_{13} is still unknown and Earth

matter effects are observed, an ambiguity between case A and C exists. In sec. 4, we discuss how this degeneracy can be broken using the information from the prompt ν_e neutronization burst.

2 Identifying signatures of the SN shock wave propagation

The neutrino spectra F_{ν_i} arriving at the Earth are determined by the primary neutrino spectra $F^0_{\nu_i}$ as well as the neutrino mixing scenario, $F_{\nu_i}(E,t) = \sum_j p_{ji}(E,t) F^0_{\nu_j}(E,t)$, where p_{ji} is the conversion probability of a ν_j into ν_i after propagation through the SN mantle. The probabilities p_{ji} are basically determined by the number of resonances that the neutrinos traverse and their adiabaticity. Both are directly connected to the neutrino mixing scheme. In contrast to the solar case, SN neutrinos must pass through two resonance layers: the H-resonance layer at $\rho_{\rm H} \sim 10^3$ g/cm^3 corresponding to $\Delta m^2_{\rm atm}$, and the L-resonance layer at $\rho_{\rm L} \sim 10$ g/cm^3 corresponding to $\Delta m^2_{\odot}$. Whereas the L-resonance is always adiabatic and in the neutrino channel, the adiabaticity of the H-resonance depends on the value of ϑ_{13}, and the resonance shows up in the neutrino or antineutrino channel for a normal or inverted mass hierarchy respectively [1].

During approximately the first two seconds after core bounce, the neutrino survival probabilities are constant in time and in energy for all three cases A, B, and C. However, at $t \approx 2$ s the H-resonance layer is reached by the outgoing shock wave, see the left panel of Fig. 1. The way the shock wave passage affects the neutrino propagation strongly depends on the neutrino mixing scenario: cases A and C will not show any evidence of shock wave propagation in the observed $\bar{\nu}_e$ spectrum, either because there is no resonance in the antineutrino channel as in scenario A, or because the resonance is always strongly non-adiabatic as in scenario C. However, in scenario B, the sudden change in the density breaks the adiabaticity of the resonance, leading to observable consequences in the $\bar{\nu}_e$ spectrum.

The key ingredient to observe signatures of the shock wave propagation is the time and energy dependence of the neutrino survival probability. In the right panel of Fig. 1, we show $\bar{p}(E,t) \equiv p_{\bar{\nu}_e \bar{\nu}_e}$ averaged with the energy resolution function of Super-Kamiokande, for the case with a forward and a reverse shock. The latters forms when a neutrino-driven baryonic wind develops and collides with the earlier, more slowly expanding SN ejecta. Although the exact propagation history depends on the detailed dynamics during the early stages of the SN explosion, a reverse shock forms in all

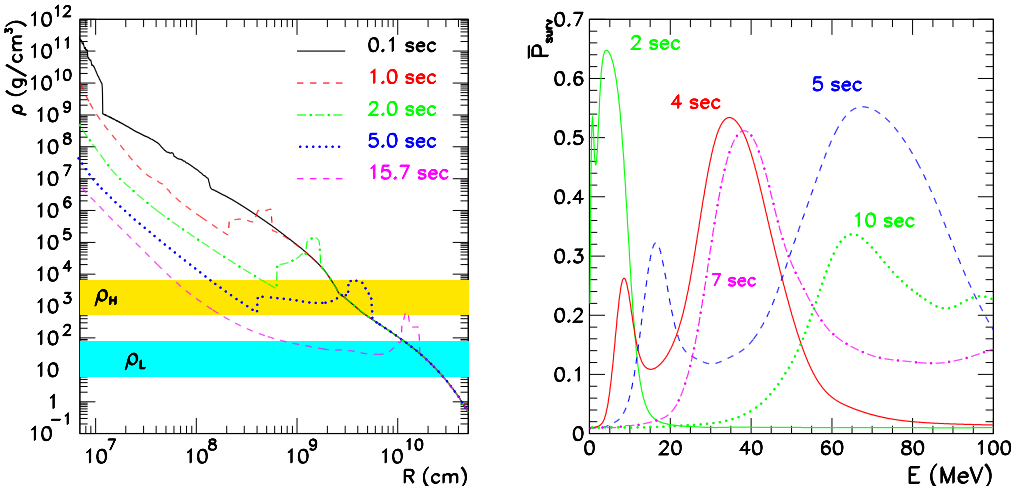

Figure 1: Left: Shock and reverse-shock propagation. The density profile is shown at the indicated instances after core bounce. The density region $\rho_{\rm H}$ corresponds to resonant neutrino oscillations with the atmospheric mass difference, $\rho_{\rm L}$ to the solar one [7]. Right: Survival probability $\bar{p}(E,t)$ as function of energy at different times [7].

models which were computed with sufficient resolution [7]. The presence of two shocks results in a dip in $\bar{p}(E,t)$ at those energies for which the resonance region is passed by both shock waves. All these structures move in time towards higher energies, as the shock waves reach regions with lower density.

A useful observable to detect effects of the shock propagation is the average of the measured positron energies, $\langle E_e \rangle$. In Fig. 2, we show $\langle E_e \rangle$ together with the one sigma errors expected for a megaton water Cherenkov detector and a SN in 10 kpc distance, with a time binning of 0.5 s: Both panels contains the case that no shock wave influences the neutrino propagation, the case of only a forward shock wave and of both forward and reverse shock wave. The left and right panels show two different models for neutrino fluxes: G1 assumes different average energies of the emitted neutrinos, $\langle E_0(\nu_x)\rangle/\langle E_0(\bar{\nu}_e)\rangle = 1.2$, and similar fluxes, $\Phi_0(\nu_e)/\Phi_0(\nu_x) = 0.8$, while G2 assumes identical energy spectra, $\langle E_0(\nu_x)\rangle/\langle E_0(\bar{\nu}_e)\rangle = 1$, and $\Phi_0(\nu_e)/\Phi_0(\nu_x) = 0.5$.

The effects of the shock wave propagation are clearly visible, independent of the assumptions about the initial neutrino spectra. Moreover, it is not only possible to detect the shock wave propagation in general, but also to identify the specific imprints of the forward and reverse shock versus the

forward shock only case. The signature of the reverse shock is its double-dip structure compared to the one-dip of a forward shock only. To study the dependence of the double-dip structure on the value of ϑ_{13}, we show $\langle E_e \rangle$ as function of time for different 13-mixing angles in the left panel of Fig. 3. Even for as small values as $\tan^2 \vartheta_{13} = 5 \times 10^{-5}$ the double-dip is still clearly visible, while for $\tan^2 \vartheta_{13} = 1 \times 10^{-5}$ only a bump modulates the neutrino signal.

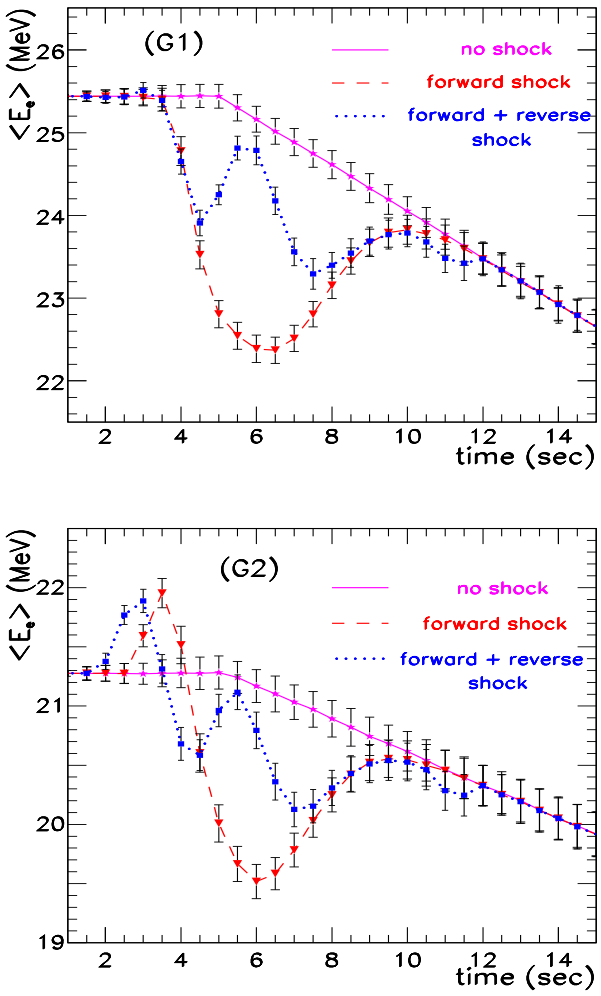

Figure 2: The average energy of $\bar{\nu}p \to ne^+$ events binned in time for a static density profile (magenta), a profile with only a forward shock (red) and with forward and reverse shock (blue). The error bars represent 1 σ errors in any bin, from Ref. [7].

In the right panel of Fig. 3, we show the number of events binned in energy intervals of 10 MeV as function of time for the case of a reverse shock. We can observe clearly how the positions of the two dips change in each energy bin. It is remarkable that the double-dip feature allows one to trace the shock propagation: Given the neutrino mixing scheme, the neutrino energy fixes the resonance density. Therefore, the progress of the shock fronts can be read off from the position of the double-dip in the neutrino spectra of different energy. Thus, the observation of shock wave effects does not only identify case B (inverted hierarchy, large ϑ_{13}), but gives also access to physics deep inside the SN.

3 Earth-matter effects

During the first two seconds after post-bounce, during which roughly half of all neutrinos are emitted, the dependence of the probability to reach the Earth on the neutrino energy E is very weak. However, if neutrinos cross the Earth before reaching the detector, p_{ij} may become energy-dependent and induce modulations in the neutrino energy spectrum. These modulations may be observed in the form of local peaks and valleys in the spectrum of the event rate $\sigma F_{\bar{e}}^D$ plotted as a function of $1/E$. These modulations arise in the antineutrino channel only in cases A and C. Therefore its observation would exclude case B. This distortion in the spectra could be measured by comparing the neutrino signal at two or more different detectors such that the neutrinos travel different distances through the Earth before reaching them [2, 8]. However these Earth matter effects can be also identified in a single detector [4, 5].

The net $\bar{\nu}_e$ flux at the detector may be written in the form

$$F_{\bar{e}}^D = \sin^2\vartheta_{12} F_{\bar{x}}^0 + \cos^2\vartheta_{12} F_{\bar{e}}^0 + \Delta F^0 \sum_{i=1}^{7} \bar{A}_i \sin^2(k_i y/2)\,, \qquad (1)$$

where y is the "inverse energy" parameter $y \equiv 12.5\,\mathrm{MeV}/E$, $\Delta F^0 \equiv (F_{\bar{e}}^0 - F_{\bar{x}}^0)$ depends only on the primary neutrino spectra, whereas the $\bar{A}_i$ depend only on the mixing parameters and are independent of the primary spectra.

The last term in Eq. (1) is the Earth oscillation term that contains up to seven analytically known frequencies k_i in y, the coefficients $\Delta F^0 \bar{A}_i$ being relatively slowly varying functions of y. The first two terms in Eq. (1) are also slowly varying functions of y, and hence contain frequencies in y that are much smaller than the k_i. The frequencies k_i are completely independent of the primary neutrino spectra, and can be determined to a good accuracy from the knowledge of the solar oscillation parameters, the Earth matter density,

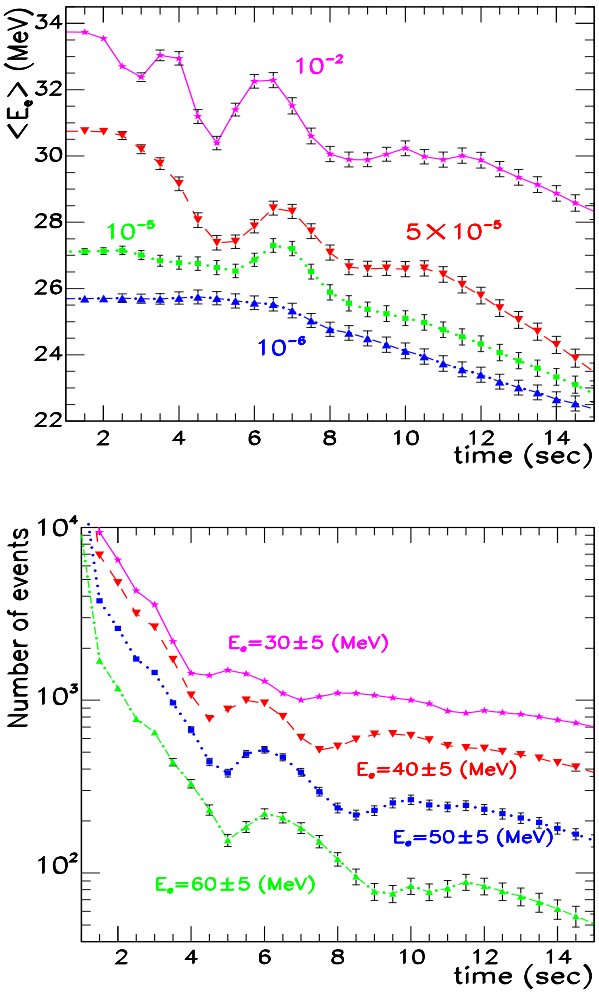

Figure 3: Left: Time dependence of $\langle E_e \rangle$ for a profile with a forward and reverse shock for several values of $\tan^2 \vartheta_{13}$ as indicated. Upper: Number of events binned per energy decade as function of time for forward and reverse shock, from Ref. [7].

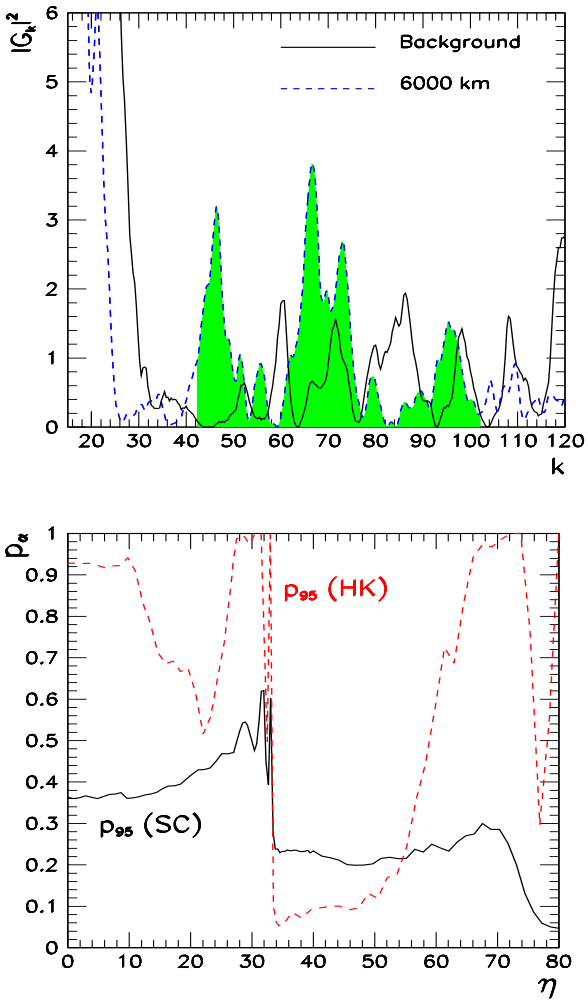

Figure 4: Upper: Realistic power spectrum from a single simulation [5]. Lower: Comparison of p_{95} as a function of nadir angle η using a "floating cut" as discussed in Ref. [5] for a 32 kton scintillator (SC) and a megaton water Cherenkov (HK) detector.

and the position of the SN in the sky [5]. The latter can be determined with sufficient precision even if the SN is optically obscured using the pointing capability of neutrino detectors [9].

The power spectrum of N detected neutrino events is

$$G(k) \equiv \frac{1}{N} \left| \sum_{i=1}^{N} e^{iky_i} \right|^2 . \tag{2}$$

In the absence of Earth effect modulations, $G(k)$ has an average value of one for $k \gtrsim 40$. The region $k \lesssim 40$ is dominated by the "0-peak," which is a manifestation of the low frequency terms in Eq. (1). Identifying Earth effects is equivalent to observing excess power in $G(k)$ around the known frequencies k_i, cf. Fig. 4. The area under the power spectrum between two fixed frequencies $k_{\rm min}$ and $k_{\rm max}$ is on an average $(k_{\rm max} - k_{\rm min})$. In the absence of Earth effects, this area will have a distribution centered around this mean. The Earth effect peaks tend to increase this area. The confidence level of peak identification, p_α, may then be defined as the fraction of the area of the background distribution that is less than the actual area measured.

In the right panel of Fig. 4, we assume the model G1 for the neutrino fluxes and compare the results obtained with a 32 kton scintillator detector and a megaton water Cherenkov detector. In the latter case, as neutrinos travel more and more distance in the mantle the peak moves to higher k values, and due to the high k suppression, the efficiency of peak identification decreases. When the neutrinos start traversing the core, additional low k peaks are generated and the efficiency increases again.

The identification of Earth matter effects excludes case B, and it thus complementary to the observation of shock wave effects.

4 Neutronization ν_e burst

The possible ambiguity between cases A and C cannot be resolved by the observation of Earth matter effects alone, if the value of ϑ_{13} is unknown. In this case, the additional information encoded in the ν_e neutrinos emitted during the neutronization burst might fix the range of ϑ_{13} as well as the neutrino mass hierarchy.

The neutronization burst lasts about 10 milliseconds and reaches a peak luminosity $L \approx 10^{53}$ erg/s. Despite this enormous luminosity, the duration of the burst is so short that the number of events expected is small. Moreover, the uncertainty of SN models is still so large that this number has a rather large incertitude [10]. However, the time-dependence of the peak is rather model-independent [11], see also the left panel of Fig. 5.

The observation of the neutronization ν_e burst as a tool for determining the neutrino parameters offers also one important advantage: during the burst, the SN is emitting essentially just neutrinos of one flavor, ν_e. Thus the observation of such a peak in a detector sensitive to ν_e via charged current reactions, like SNO or liquid Ar detectors, would rule out case A (where $p_{\nu_e\nu_e} \approx 0$) [11, 12].

For an identification of the neutronization burst, it is necessary to follow the time evolution of the peak, instead of simply considering the total number of events in the early-phase of the SN: the latter is too model-dependent and should be therefore not used as observable. Binning the events in time requires however a large enough number of events, and therefore we consider instead of SNO the case of a megaton water Cherenkov detector.

Main background to the reaction we are interested in, elastic scattering of ν_e on electrons, are inverse beta decays $\bar{\nu}_e p \to n e^+$. It can be strongly reduced by using a cut in the forward direction and/or by tagging it with Gadolinium. The irreducible background comes from the other elastic scattering reactions on electrons, namely from ν_x via neutral current and $\bar{\nu}_e$. Therefore we consider as observable the number of all elastic scattering events on electrons.

In the right panel of Fig. 5, we plot the number of elastic scattering events in five time bins for two SN models with 13 and $25 M_\odot$ progenitor masses, and for the cases A and C. Although all neutrino flavors contribute to the observable, the method turns out to be rather powerful in disentangle A and C: While in the case C a clear peak structure is visible, with a significant decrease in the number of events in the fourth bin, in case A this structure is practically absent.

Thus the detection of the neutronization ν_e peak breaks the degeneracy between A and C for unknown ϑ_{13}. The model-dependence of the absolute values of the neutrino fluxes can be avoided, if enough events are observed so that the peak structure of the neutronization burst can be resolved.

5 Summary

A reliable determination of neutrino parameters using SN neutrinos should be independent from our poor understanding of the primary neutrino fluxes produced inside the SN. Earth-matter effects and the passage of SN shocks through the H-resonance both introduce unique modulations in the neutrino energy spectrum that allow one their identification without knowledge of the primary neutrino spectra. While the observation of Earth-matter effects in the $\bar{\nu}_e$ energy spectrum rules out case B, modulations in the $\bar{\nu}_e$ time spectrum

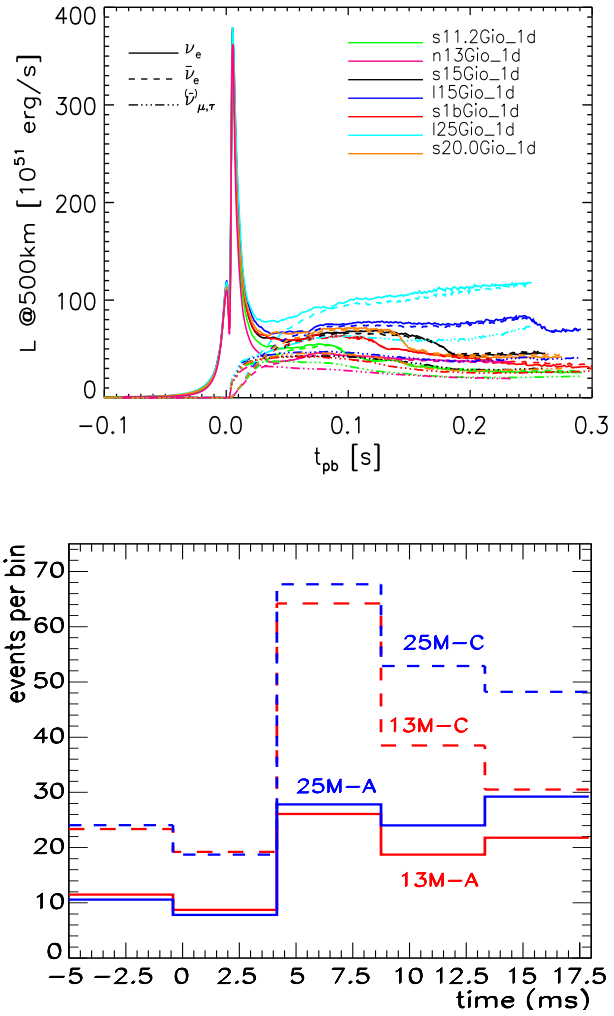

Figure 5: Upper: Neutrino luminosities as function of time for different progenitor masses, from [13]. Lower: Event number expected in megaton water Cherenkov detector binned in time.

identify case B. If the value of ϑ_{13} would be know to be large, then the neutrino mass hierarchy would be identified. Otherwise, the detection of the neutronization ν_e peak can break the remaining degeneracy between A and C.

Acknowledgments

We would like to thank our co-authors A. S. Dighe, G. G. Raffelt, H.-T. Janka and L. Scheck for many useful discussions and pleasant collaborations, R. Buras and H.-T. Janka for discussions about the neutronization burst and for providing data, and T. Schwetz for helpful comments about the manuscript. MK acknowledges support by an Emmy-Noether grant of the Deutsche Forschungsgemeinschaft, and RT a Marie-Curie-Fellowship of the European Community.

References

[1] A. S. Dighe and A. Y. Smirnov, Phys. Rev. D **62**, 033007 (2000).

[2] C. Lunardini and A. Y. Smirnov, Nucl. Phys. B **616**, 307 (2001).

[3] K. Takahashi and K. Sato, Prog. Theor. Phys. **109**, 919 (2003); C. Lunardini and A. Y. Smirnov, JCAP **0306**, 009 (2003).

[4] A. S. Dighe, M. T. Keil and G. G. Raffelt, JCAP **0306**, 006 (2003).

[5] A. S. Dighe *et al.*, JCAP **0401**, 004 (2004).

[6] R. C. Schirato and G. M. Fuller, astro-ph/0205390; G. L. Fogli, E. Lisi, D. Montanino and A. Mirizzi, Phys. Rev. D **68**, 033005 (2003).

[7] R. Tomàs *et al.*, [astro-ph/0407132].

[8] A. S. Dighe, M. T. Keil and G. G. Raffelt, JCAP **0306**, 005 (2003).

[9] R. Tomàs *et al.*, Phys. Rev. D **68**, 093013 (2003).

[10] See for instance W. R. Hix *et al.*, Phys. Rev. Lett. **91**, 201102 (2003).

[11] K. Takahashi, K. Sato, A. Burrows and T. A. Thompson, Phys. Rev. D **68**, 113009 (2003).

[12] I. Gil-Botella and A. Rubbia, JCAP **0310**, 009 (2003).

[13] R. Buras and H.-T. Janka, private communication.